Performance Improvement for Constellation SAR using Signal Processing Techniques

ZHENFANG LI

ZHENG BAO, Senior Member, IEEE

HONGYANG WANG

GUISHENG LIAO, Member, IEEE
Xidian University
China

A new concept of spaceborne synthetic aperture radar (SAR) implementation has recently been proposed—the constellation of small spaceborne SAR systems. In this implementation, several formation-flying small satellites cooperate to perform multiple space missions. We investigate the possibility to produce high-resolution wide-area SAR images and fine ground moving-target indicator (GMTI) performance with constellation of small spaceborne SAR systems. In particular, we focus on the problems introduced by this particular SAR system, such as Doppler ambiguities, high sparseness of the satellite array, and array element errors. A space-time adaptive processing (STAP) approach combined with conventional SAR imaging algorithms is proposed which can solve these problems to some extent. The main idea of the approach is to use a STAP-based method to properly overcome the aliasing effect caused by the lower pulse-repetition frequency (PRF) and thereby retrieve the unambiguous azimuth wide (full) spectrum signals from the received echoes. Following this operation, conventional SAR data processing tools can be applied to focus the SAR images fully. The proposed approach can simultaneously achieve both high-resolution SAR mapping of wide ground scenes and GMTI with high efficiency. To obtain array element errors, an array auto-calibration technique is proposed to estimate them based on the angular and Doppler ambiguity analysis of the clutter echo. The optimizing of satellite formations is also analyzed, and a platform velocity/PRF criterion for array configurations is presented. An approach is given to make it possible that almost any given sparse array configuration can satisfy the criterion by slightly adjusting the PRF. Simulated results are presented to verify the effectiveness of the proposed approaches.

Manuscript received January 2, 2004; revised July 13, 2005; released for publication September 14, 2005.

IEEE Log No. T-AES/42/2/876423.

Refereeing of this contribution was handled by P. Lombardini.

Authors' current addresses: Z. Li, Z. Bao, G. Liao, National Lab of Radar Signal Processing, Xidian University, Xi'an 710071, China, E-mail: (LZF@xidian.edu.cn); H. Wang, Chinese University of Hong Kong, China.

I. INTRODUCTION

A new conceptual implementation of spaceborne synthetic aperture radar (SAR) systems was proposed by Air Force Research Laboratory (AFRL) in 1997 [1, 2], that is, the constellation implementation of small spaceborne SAR systems. In this implementation, several small satellites (or micro-satellites) fly in a formation and operate as a single "virtual satellite."

Constellation SAR systems have many advantages over conventional spaceborne SAR systems. They can provide multiple, long baselines in single-pass observation mode, thus greatly improving the performance of interferometric SAR (InSAR) and ground moving-target indicator (GMTI). The coherent combination of several SAR images obtained from different observing angles can improve the image resolution and provide accurate geometric information [3, 4]. Furthermore, combining a broad illumination source with multiple small receiving antennas placed on separate formation-flying micro-satellites, we can obtain high-resolution SAR images of wide areas [5–7]. Another reason for using the constellation SAR systems is to mitigate the cost, fabrication, and deployment issues associated with placing a large satellite SAR into orbit [5]. Furthermore, the likelihood of system failure can be reduced since failure generally occurs only to individual micro-satellites, instead of a large satellite carrying an entire system.

However, several challenging problems are also introduced by the constellation SAR regime at the same time. These problems should be carefully considered when building the constellation SAR system. The following briefly reviews these problems and introduces the corresponding solutions.

A. Highly Sparse Array

Due to the high sparseness of the distributed satellite array (to avoid the risk of collision, the interval between any two satellites must be at least 100 m) and the limited number of satellites, the beam pattern formed by this array will have high sidelobe levels and even grating lobes which can degrade the performance of GMTI (i.e., they can cause excessive "blind speed" regions in which ground moving targets cannot be detected). It is challenging work to use this highly sparse array to suppress the clutter and detect ground moving targets with fine speed response.

A method for improving the beam pattern is that each satellite respectively transmits an orthogonal signal (multi-frequency/coded signal), and the echoes from every satellite's transmission are coherently processed [1]. A technique of pattern synthesis in angle-frequency space for GMTI has been proposed in [8] which requires that all satellites be spaced

regularly to achieve regular grating lobes distribution. A so-called scanned pattern interferometric radar (SPIR) approach has been proposed in [9] which uses the high angular variability of a sparse array point spread function (PSF) to collect sufficient data from the ground return so that the clutter and ground moving targets can be separated without a priori assumption of the clutter statistics. The displaced phase center antenna (DPCA) technique can also be used to cancel the clutter [10, 11]. Unfortunately, if the DPCA condition is met, the satellite formation cannot be used to resolve the clutter Doppler ambiguities for unambiguous SAR imaging of ground scenes (the detailed explanation is given in Section V).

In this paper we first use temporal processing (temporal degrees of freedom) to divide the echo spectra into many short chips (all of the chips occupying the same Doppler frequency are within the same Doppler bin). Thus, within each Doppler bin, each of the spectrum chips (including those of the clutter and ground moving targets) is confined into a narrow angle space; these spectrum chips are completely separated from each other in spatial domain (angle domain). Then we can easily use spatial beamforming techniques (even for the highly sparse array) to process the spectrum chips.

B. Range/Doppler Ambiguities

A basic limitation for the design of spaceborne SAR systems is the minimum antenna area constraint [12–15] which can be expressed as

$$A_{\min} = 4v_s\lambda r \cdot \tan\varphi / c \tag{1}$$

where v_s is the velocity of spaceborne platforms, λ is the wavelength, r is the slant range, c is the light speed, and φ is the incidence angle. The requirement arises because the illuminated area of the ground must be restricted so that the radar does not receive ambiguous returns in range or/and Doppler. As a result, all of the current spaceborne SAR systems have huge antennas, such as ERS-1/2 (with antenna aperture of 10 m $\times$ 1 m), Radarsat-1 (with antenna aperture of 15 m $\times$ 1.5 m), and SIR-C/X-SAR (with antenna aperture of 12 m $\times$ 4.4 m). Unfortunately, a large antenna leads to the failure of the conventional spaceborne SAR systems to map a wide area with high azimuth resolution either in the stripmap or spotlight mode. On the other hand, it is impractical to put such a large radar antenna on a micro-satellite platform. Therefore the minimum antenna area constraint cannot be satisfied by individual small antennas. However, we should emphasize that the total receiving antenna area (i.e., the sum of all physical receiving aperture areas) in the constellation must satisfy the minimum antenna area constraint to obtain unambiguous fine-quality SAR images, which is assumed here. Under this assumption we investigate approaches to wide-swath and high-resolution SAR image generation from the constellation of small spaceborne SAR systems. Since an individual antenna does not meet the minimum antenna area constraint, the range and/or Doppler ambiguities will be introduced into the echoes received by each satellite. To avoid range ambiguity, a lower PRF is assumed throughout this paper, so we only need to overcome the Doppler ambiguity effects.

The maximum likelihood (ML) filter and minimum mean-squared error (MMSE) filter (using the entire time, frequency, and spatial measurements) have been used to resolve the problem of the range-Doppler ambiguities and to achieve the wide-area SAR image [5]. However, calculating the ML and MMSE filters would require the inversion of an extremely large matrix, which is unrealistic. The authors of [5] have also suggested that the SAR processing be first performed for each receiving channel, and then spatial processing be used to reject ambiguous targets for each image pixel. However, several problems still remain unsolved, such as heavy computational burden (due to the multiplication of SAR processing by the number of satellites) and more spatial degrees of freedom required to reject the more ambiguous targets (the number of ambiguous targets within each pixel is twice the number of Doppler ambiguities, see [6]) within each pixel of the full-resolution SAR images. A reconstruction algorithm based on the sampling theorem has been investigated to recover the unambiguous Doppler spectrum [6]. Aguttes has introduced a totally different approach to solve the problems of the Doppler ambiguity and nonuniform spaced satellites by using spread spectrum waveforms [7].

In this paper we present a novel STAP-based approach to resolve the Doppler ambiguities by retrieving the unambiguous full spectrum of the clutter and wide spectra of ground moving targets. Thus the ground moving target signals can be separated from the clutter. Then conventional SAR data processing tools can be directly applied to focus fully the SAR images of ground scenes and ground moving targets. Using this approach, we can simultaneously achieve the unambiguous high-resolution SAR images of wide areas and GMTI with high efficiency.

C. Array Element Errors

To combine the echoes coherently from every satellite, we need to know the array manifold exactly. However, it is almost impossible for the current measurement techniques to collect the information of each array element accurately, such as gain-phase error, position uncertainties, timing uncertainty, etc.,

especially for the highly sparse satellite array with operating frequency at X band.

A data-dependent array auto-calibration technique is proposed here to estimate the array element errors based on the space-time analysis of the clutter echo, which possesses both the advantages (such as fast convergence) of source-calibrations [16, 17] and those (such as no need for artificial pilot sources) of self calibrations [18, 19]. As mentioned above, the clutter echo has multiple Doppler ambiguities; the clutter spectrum chips (after processed by using azimuth fast Fourier transform (FFT)) within a Doppler bin are used as the array calibration sources in our array calibration technique. To distinguish the different error contributions to array steering vectors, we model the three-dimensional position errors as two phase errors. One is fixed for all echoes from the antenna main beam; thus it can be incorporated into the inherent element gain-phase error. The other is variable for different spectrum chips; therefore it must be estimated, respectively, for different spectrum chips. If the timing uncertainty can also be modeled as a fixed phase error, the auto-calibration technique here can also provide an estimation of the timing uncertainty. The proposed array auto-calibration technique can converge quickly, and the corresponding computational burden can be extremely decreased.

The succeeding sections of this paper are arranged as follows. Section II presents the mathematical model and characteristics of echoes. In Section III, the processing approach to SAR and GMTI is presented in detail. The array auto-calibration technique is presented in Section IV. The satellite formation optimization is discussed in Section V. Section VI shows the simulated results with our conclusions in Section VII.

II. ECHO MODEL

A. Coordinate System

The coordinate system of a constellation is defined as follows: X-axis is in the direction of the satellite (reference satellite) velocity vector; Z-axis is away from the center of the Earth; Y-axis is along the orbital angular momentum vector. The (X, Y, Z) directions can also be referred to as (along-track, cross-track, radial) or (front, left, up). The spaceborne SAR systems usually look at the right side. The coordinate system is shown in Fig. 1. The angles θ, φ, and ϕ shown in Fig. 1 are referred to as the azimuth angle, incidence angle, and cone angle, respectively, and their relation can be given by

$$\sin\phi = \sin\theta\sin\varphi. \tag{2}$$

The Earth is assumed to be stationary in this coordinate system, i.e., the coordinate system is an

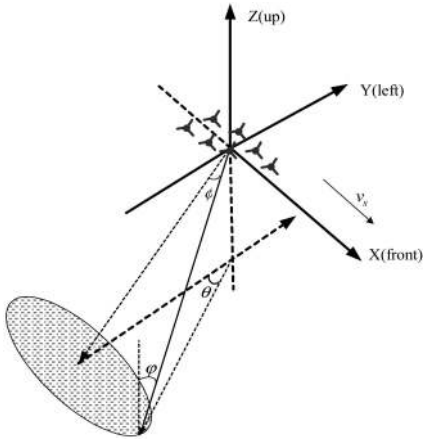

Fig. 1. Coordinate system of constellation SAR systems.

Earth reference frame. To simplify the analysis, we assume that all satellites in the constellation only have an identical along-track velocity v_s. In fact, the other velocity components are very small relative to the along-track velocity if appropriately designing the orbits [7], and the effects caused by them can also be easily compensated. The objective of the work presented here is to present our processing approaches in an easy manner, so these practical considerations are neglected temporarily.

To simplify the mathematical model, it is important to give the definition of equivalent phase center firstly.

DEFINITION Two separate transmitting and receiving antennas can be equivalent to one transmitting and receiving antenna, defined as the equivalent phase center herein, which is located at the midpoint between the separate transmitting and receiving antennas, after compensating a constant phase $\exp\{j2\pi d^2/(4r\lambda)\}$ (where d is the distance between the transmitting and receiving antennas, r is the slant range from the equivalent phase center to the illuminated ground surface, and λ is the wavelength). In practice, the phase compensation can be performed for range segments one by one. In each range segment, the phase factor can be approximated to be a constant, i.e., r can be approximated to be constant. This definition holds only when the distance between transmitter and receiver is small enough compared with their distance to the surface of the Earth. It is assumed here that this definition is valid for typical constellation SAR system parameters. For example, even if the distance between transmitting and receiving antennas is as large as 1000 m, the maximum phase error caused by this approximation is still less than 1° for typical spaceborne SAR system parameters (as listed in Table I).

Based on the definition of equivalent phase center, it is assumed throughout this paper that the coordinates of each satellite are given according to its equivalent phase center, i.e., each equivalent phase

center serves as both transmitter and receiver, although only one satellite is used as the transmitter in the constellation.

B. Mathematical Model

Assume that the coordinates of the mth ($m = 1,2,\ldots,M$ and M is the number of satellites in the constellation) satellite are (x_m, y_m, z_m) at time $t = 0$ (for the reference satellite, its coordinates are $(x_1, y_1, z_1) = (0,0,0)$), and $(x_m + v_s t, y_m, z_m)$ (v_s is the satellite along-track velocity) at time t. The clutter echo received by the mth satellite at time t can be written as

$$s_{c,m}(\tau,t) = \iint \sigma(x,y) h\left(\tau - \frac{2r_{c,m}(x,y,z,t)}{c}\right) \times g\left(t - \frac{x - x_m}{v_s}\right) e^{-j4\pi r_{c,m}(x,y,z,t)/\lambda} dx\,dy \tag{3}$$

where

$$r_{c,m}(x,y,z,t) = \sqrt{(x - x_m - v_s t)^2 + (y - y_m)^2 + (z(x,y) - z_m)^2} \tag{4}$$

$$h(\tau) = a(\tau) e^{-j\pi k_r \tau^2} \tag{5}$$

and t and τ denote the azimuth slow-time and range fast-time, respectively, c is the light velocity, λ is the wavelength of the carrier, $\sigma(x,y)$ is the complex reflectivity per unit area (surface scattering) at a ground reflecting cell whose coordinates are $(x,y,z(x,y))$ (in the following, we directly use the notation z instead of $z(x,y)$), $r_{c,m}(x,y,z,t)$ is the slant range from the equivalent phase center of the mth satellite to the ground cell, $h(\tau)$ is the complex transmitted pulse (linear FM waveform), $a(\tau)$ is the complex envelope of the transmitted pulse, and $g(t)$ represents the antenna pattern and other time-variant characters (identical to all the receiving antennas).

Assume that the constellation SAR system operates in the side-looking mode, and the along-track length of the illuminated ground region is significantly less than the slant range, i.e., $r_{c,m}(x,y,z,t) \gg |x - v_s t - x_m|$. Moreover, we assume here that y_m and z_m are as small as possible, such as only 10 m or smaller (i.e., the SAR train as called in [7]). Thus $r_{c,m}(x,y,z,t)$ can be approximated as

$$\begin{aligned} r_{c,m}(x,y,z,t) &\approx \frac{-y \cdot y_m}{\sqrt{(x - x_m - v_s t)^2 + y^2 + z^2}} + \frac{-z \cdot z_m}{\sqrt{(x - x_m - v_s t)^2 + y^2 + z^2}} + \sqrt{y^2 + z^2} + \frac{(x - v_s t - x_m)^2}{2\sqrt{y^2 + z^2}} \\ &= -y_m \cos\theta_{c,m}(x,y,z,t) \sin\varphi_{c,m}(x,y,z,t) - z_m \cos\varphi_{c,m}(x,y,z,t) + \sqrt{y^2 + z^2} + \frac{(x - v_s t - x_m)^2}{2\sqrt{y^2 + z^2}} \end{aligned} \tag{6}$$

where

$$\begin{aligned} \sin\theta_{c,m}(x,y,z,t) &= \frac{x - x_m - v_s t}{\sqrt{(x - x_m - v_s t)^2 + y^2}} \approx \frac{x - x_m - v_s t}{|y|} \\ \sin\varphi_{c,m}(x,y,z,t) &= \frac{\sqrt{(x - x_m - v_s t)^2 + y^2}}{\sqrt{(x - x_m - v_s t)^2 + y^2 + z^2}} \approx \frac{|y|}{\sqrt{y^2 + z^2}} \triangleq \sin\varphi_c(x,y,z). \end{aligned} \tag{7, 8}$$

and $\theta_{c,m}(x,y,z,t)$ and $\varphi_{c,m}(x,y,z,t)$ are the instantaneous azimuth and incidence angles (as shown in Fig. 1) of the clutter cell (x,y,z) relative to the mth satellite, respectively. The error can be neglected for typical spaceborne SAR system parameters.

Using (6) in (3) gives

$$s_{c,m}(\tau,t) = \iint \sigma(x,y) h\left(\tau - \frac{2r_{c,m}(x,y,z,t)}{c}\right) \times g\left(t - \frac{x - x_m}{v_s}\right) e^{-j\psi_{c,m}(x,y,z,t)} dx\,dy \tag{9}$$

where

$$\begin{aligned} \psi_{c,m}(x,y,z,t) &= \frac{4\pi}{\lambda}(-y_m \cos\theta_{c,m}(x,y,z,t) \sin\varphi_c(x,y,z) - z_m \cos\varphi_c(x,y,z)) + \frac{4\pi}{\lambda}\sqrt{y^2 + z^2} + \frac{2\pi v_s^2 \left(t - \frac{x - x_m}{v_s}\right)^2}{\lambda\sqrt{y^2 + z^2}}. \end{aligned} \tag{10}$$

We can see from (10) that the echo signal from the clutter cell at (x,y,z) is also a linear FM signal in the azimuth time domain with the azimuth chirp rate of

$$k_{dm}(x,y,z) = -\frac{2v_s^2}{\lambda\sqrt{y^2 + z^2}}. \tag{11}$$

Using (11), the instantaneous Doppler frequency $f_{dm}(x,y,z,t)$ of the clutter cell at (x,y,z) relative to the mth antenna can be expressed as

$$\begin{aligned} f_{dm}(x,y,z,t) &= k_{dm}(x,y,z)\left(t - \frac{x - x_m}{v_s}\right) \\ &= -\frac{2v_s^2}{\lambda\sqrt{y^2 + z^2}}\left(t - \frac{x - x_m}{v_s}\right). \end{aligned} \tag{12}$$

According to (12) we can obtain the instantaneous azimuth time $t_m(x,y,z,f_d)$ corresponding to the

Doppler frequency f_d as

$$t_m(x,y,z,f_d) = \frac{x-x_m}{v_s} - \frac{\lambda\sqrt{y^2+z^2}}{2v_s^2} f_d. \tag{13}$$

Using (13) in (7) gives

$$\begin{aligned}\sin\theta_{c,m}(x,y,z,f_d) &= \frac{\lambda\sqrt{y^2+z^2}}{2v_s|y|} f_d \\ &= \frac{\lambda}{2v_s\sin\varphi_c(x,y,z)} f_d \\ &\triangleq \sin\theta_c(x,y,z,f_d).\end{aligned} \tag{14}$$

$\theta_c(x,y,z,f_d)$ denotes the instantaneous azimuth angle of the clutter cell (x,y,z) relative to each satellite (i.e., identical to all satellites) when the instantaneous Doppler frequency is f_d. If the illuminated ground is flat (or y_m and z_m are very small), we can directly obtain $\varphi_c(x,y,z)$ (or by approximating) according to the range bin τ. That is, if the range-Doppler bin $\tau - f_d$ is given, the incidence angle $\varphi_c(x,y,z)$ and the azimuth angle $\theta_c(x,y,z,f_d)$ can be calculated according to (8) and (14), respectively. The incidence angle and the azimuth angle are independent of the along-track position of each clutter cell, i.e., all the clutter cells within the same range-Doppler bin have (approximately) identical azimuth and incidence angles. Therefore, for the sake of simplicity, we use the notations $\varphi_c(\tau)$ (instead of $\varphi_c(x,y,z)$) and $\theta_c(\tau,f_d)$ (instead of $\theta_c(x,y,z,f_d)$) to denote the azimuth and incidence angles corresponding to the range-Doppler bin $\tau - f_d$, respectively.

Transforming (9) into the Doppler domain (using the stationary phase method), we can obtain

$$S_{c,m}(\tau,f_d) = e^{j(4\pi/\lambda)d_{c,m}(\tau,f_d)} A_{c,m}(\tau,f_d) \tag{15}$$

where

$$A_{c,m}(\tau,f_d) = \int\!\!\int S'_{c,m}(x,y,z,f_d)\,dx\,dy \tag{16}$$

$$\begin{aligned}S'_{c,m}(x,y,z,f_d) &= \sigma(x,y)h\left(\tau - \frac{2r_{c,m}(x,y,z,f_d)}{c}\right) \\ &\quad\times G(f_d)e^{-j\psi'_c(x,y,z,f_d)}\end{aligned} \tag{17}$$

$$\psi'_c(x,y,z,f_d) = 2\pi f_d\frac{x}{v_s} + \frac{4\pi}{\lambda}\sqrt{y^2+z^2} - \frac{\pi\lambda\sqrt{y^2+z^2}}{2v_s^2} f_d^2 \tag{18}$$

$$\begin{aligned}d_{c,m}(\tau,f_d) &= x_m\sin\theta_c(\tau,f_d)\sin\varphi_c(\tau) \\ &\quad + y_m\cos\theta_c(\tau,f_d)\sin\varphi_c(\tau) + z_m\cos\varphi_c(\tau)\end{aligned} \tag{19}$$

$$\begin{aligned}r_{c,m}(x,y,z,f_d) &= -y_m\cos\theta_c(\tau,f_d)\sin\varphi_c(\tau) - z_m\cos\varphi_c(\tau) \\ &\quad + \sqrt{y^2+z^2} + \frac{\lambda^2\sqrt{y^2+z^2}f_d^2}{8v_s^2}\end{aligned} \tag{20}$$

and $G(f_d)$ is the Fourier transform of $g(t)$ and $r_{c,m}(x,y,z,f_d)$ (substituting (13) into (6)) denotes the slant range from the clutter cell (x,y,z) to the mth antenna when the instantaneous Doppler frequency is f_d. Because $r_{c,m}(x,y,z,f_d)$ are different for different satellites, we must coregister the clutter echoes received by all satellites before performing the following coherent processing. We can easily coregister the clutter echoes by shifting the range-Doppler output $S_{c,m}(\tau,f_d)$ of the mth satellite by $y_m\cos\theta_c(\tau,f_d)\sin\varphi_c(\tau) + z_m\cos\varphi_c(\tau)$ in the range direction. After envelope is coregistered, the following relationships will hold:

$$\begin{aligned}r_{c,1}(x,y,z,f_d) &= r_{c,2}(x,y,z,f_d) = \cdots = r_{c,M}(x,y,z,f_d) \\ &\triangleq r_c(x,y,z,f_d)\end{aligned} \tag{21}$$

$$A_{c,1}(\tau,f_d) = A_{c,2}(\tau,f_d) = \cdots = A_{c,M}(\tau,f_d) \triangleq A_c(\tau,f_d). \tag{22}$$

As a result, there is only one phase difference $\left(e^{j(4\pi/\lambda)d_{c,m}(\tau,f_d)}\right)$ between the mth satellite and the reference satellite from the same range-Doppler bin output. It is important to note that the first term in the right side of (19) dose not arise from the plane wave approximation. In other words, even if x_m is as large as possible, (19) will still be valid. Since only one satellite is used as the illuminator and all the satellites operate in the side-looking mode, we must restrict the along-track baseline lengths to ensure that the beams of all the satellites can share enough common regions. However, the second and third terms do arise from the plane wave approximation which requires that y_m and z_m must be as small as possible (such as 10 m). We can note from (15) that there are numerous ground clutter cells within each range-Doppler bin $\tau - f_d$, and they have the identical azimuth angle $\theta_c(\tau,f_d)$ and incidence angle $\varphi_c(\tau)$, i.e., the identical array steering vector $\left[1, e^{j(4\pi/\lambda)d_{c,2}(\tau,f_d)}, \ldots, e^{j(4\pi/\lambda)d_{c,M}(\tau,f_d)}\right]^{\mathrm{T}}$ (where $(\,)^{\mathrm{T}}$ denotes the vector transpose operator). Therefore, we can simultaneously process all the ground clutter cells within each range-Doppler bin using array processing techniques.

The echo from a ground moving target can be written as

$$\begin{aligned}s_{t,m}(\tau,t) &= \sigma_t h\left(\tau - \frac{2r_{t,m}(x,y,z,t)}{c}\right) \\ &\quad\times g\left(t - \frac{x-x_m}{v_s}\right) e^{-j4\pi r_{t,m}(x,y,z,t)/\lambda}\end{aligned} \tag{23}$$

where σ_t is the complex reflecting magnitude (RCS) of the ground moving target and $r_{t,m}(x,y,z,t)$ is the slant range from the mth satellite to the ground moving target at (x,y,z). We can write $r_{t,m}(x,y,z,t)$ as

$$\begin{aligned}r_{t,m}(x,y,z,t) &= \sqrt{(x-x_m-v_st-v_{at}t)^2 + (y-y_m)^2 + (z-z_m)^2} \\ &\quad - v_{ct}t\cos\phi_{c,m}(x,y,z,t)\end{aligned} \tag{24}$$

where v_{at} and v_{ct} are the along-track and cross-track velocities of the ground moving target, respectively. Similarly as what we have done for the clutter echo, we also transform (23) into the Doppler domain and coregister the echo envelopes; then we can obtain

$$S_{t,m}(\tau, f_d) = e^{j(4\pi/\lambda)d_{t,m}(\tau,f_d)} A_t(\tau, f_d) \tag{25}$$

where

$$A_t(\tau, f_d) = \sigma_t h\left(\tau - \frac{2r_t(x,y,z,f_d)}{c}\right) G_t(f_d) e^{-j\psi_t'(x,y,z,f_d)} \tag{26}$$

$$\begin{aligned} d_{t,m}(\tau, f_d) &= x_m \sin\theta_t(\tau, f_d)\sin\varphi_t(\tau) \\ &\quad + y_m \cos\theta_t(\tau, f_d)\sin\varphi_t(\tau) + z_m \cos\varphi_t(\tau) \end{aligned} \tag{27}$$

$$G_t(f_d) = G\left(f_d - \frac{2v_{ct}\cos\phi_t(\tau, f_d)}{\lambda}\right) \tag{28}$$

$$\begin{aligned} \psi_t'(x,y,z,f_d) &= 2\pi\left(f_d - \frac{2v_{ct}\cos\phi_t(\tau,f_d)}{\lambda}\right)\frac{x}{v_s + v_{at}} \\ &\quad + \frac{4\pi}{\lambda}\sqrt{y^2+z^2} - \frac{\pi\lambda\sqrt{y^2+z^2}}{2(v_s+v_{at})^2} \\ &\quad \times \left(f_d - \frac{2v_{ct}\cos\phi_t(\tau,f_d)}{\lambda}\right)^2 \end{aligned} \tag{29}$$

$$r_t(x,y,z,f_d) \approx r_c\left(x,y,z,f_d - \frac{2v_{ct}\cos\phi_t(\tau,f_d)}{\lambda}\right) \tag{30}$$

$$\theta_t(\tau, f_d) \approx \theta_c\left(\tau, f_d - \frac{2v_{ct}\cos\phi_t(\tau,f_d)}{\lambda}\right) \tag{31}$$

$$\varphi_t(\tau) = \varphi_c(\tau) \tag{32}$$

$$\phi_t(\tau, f_d) \approx \phi_c\left(\tau, f_d - \frac{2v_{ct}\cos\phi_c(\tau,f_{dc})}{\lambda}\right) \tag{33}$$

and f_{dc} ($f_{dc} = 0$ in the side-looking mode) is the clutter Doppler center frequency.

The outputs from the range-Doppler bin $\tau - f_d$ may include the clutter, the noise, and possibly a ground moving target, which can be written in a simple form as follows:

$$\begin{aligned} S_m(\tau, f_d) &= S_{c,m}(\tau, f_d) + S_{t,m}(\tau, f_d) + n_m(\tau, f_d) \\ &= e^{j(4\pi/\lambda)d_{c,m}(\tau,f_d)} A_c(\tau, f_d) \\ &\quad + e^{j(4\pi/\lambda)d_{t,m}(\tau,f_d)} A_t(\tau, f_d) + n_m(\tau, f_d) \end{aligned} \tag{34}$$

where $n_m(\tau, f_d)$ is the additive complex white noise. It is the phase terms in (34) that are used in the following spatial processing.

C. Characteristics of Echoes

Before presenting the processing approaches, it is helpful to first introduce the characteristics of echoes (including the clutter and ground moving targets) received by each small antenna.

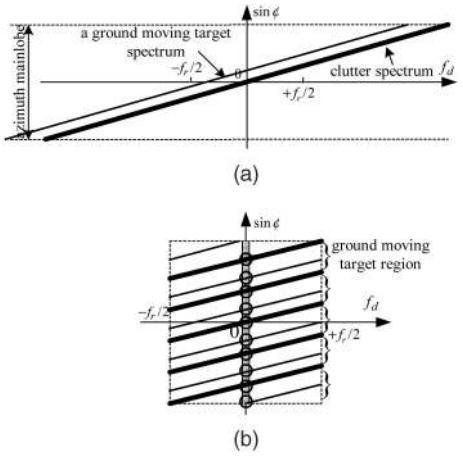

Fig. 2. Space-time spectra of clutter and ground moving target. (a) Unambiguous. (b) Doppler-ambiguous.

When a spaceborne SAR system operates in the side-looking mode, the relation (i.e., (14)) between the Doppler frequency f_d of a ground clutter cell and the corresponding cone angle ϕ (in order to simplify the equations, we substitute the notation ϕ for $\phi_c(\tau, f_d)$) can be given by

$$f_d = 2v_s \sin\phi/\lambda. \tag{35}$$

Assume that the azimuth mainlobe width of an individual small antenna equals 0.015 rad, the satellite velocity v_s = 7000 m/s, and the wavelength λ = 3 cm; then the clutter Doppler frequency coming from the antenna mainlobe is confined within [−3500 Hz, +3500 Hz]. The clutter Doppler frequency f_d is directly proportional to $\sin\phi$, so the clutter spectrum can be shown by the thick line in the f_d-$\sin\phi$ plane (also referred to as the space-time plane) of Fig. 2(a).

The PRF f_r is determined by the total receiving antenna length (i.e., the sum of the physical receiving antenna lengths) L_{total} in azimuth, and it must satisfy

$$f_r \geq 2v_s/L_{\text{total}}. \tag{36}$$

To avoid range ambiguity, a lower PRF such as f_r = 1400 Hz is assumed here. The lower PRF will introduce azimuth (Doppler) ambiguities. In this example, there will exist five azimuth angles for the same Doppler frequency, as shown by the five thick lines in Fig. 2(b). We cannot obtain a satisfactory SAR image without resolving the Doppler ambiguities.

For a ground moving target, its Doppler frequency f_d and cone angle ϕ are related by the following equation:

$$f_d = \frac{2(v_s + v_{at})}{\lambda}\sin\phi + \frac{2v_{ct}\cos\phi}{\lambda}. \tag{37}$$

The second term in the right side of (37) is an additional Doppler frequency shift caused by the cross-track motion of the ground moving target. This term indicates that for the same cone angle ϕ, the

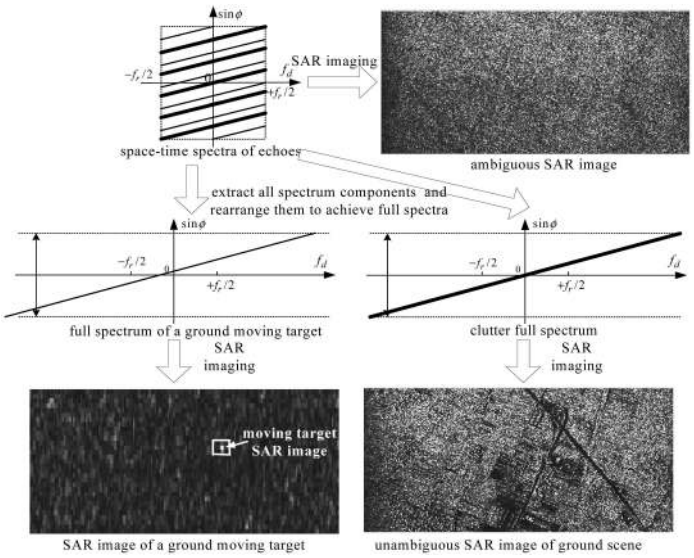

Fig. 3. Processing procedures for unambiguous SAR mapping of ground scenes and GMTI.

Doppler frequency of the ground moving target has an additional offset relative to that of the clutter; in other words, for the same Doppler frequency f_d, the ground moving target is at a different cone angle from the clutter. The spaceborne SAR system has some features which can be used to simplify the processing of GMTI. First, the satellite velocity is very high. Assuming that the satellite velocity $v_s = 7000$ m/s, the slant range $r = 1000$ km, the wavelength $\lambda = 0.03$ m, and the antenna length (in azimuth) $D = 2$ m, then the full aperture time illuminating a ground moving target is only $r\lambda/(v_s D) \approx 2$ s. Thus, we can make the assumption that the velocity of a ground target does not change during the whole dwell time. Second, the azimuth mainlobe width is so narrow that the second term in the right side of (37) can be approximated as a constant term in the side-looking mode. Third, the Doppler chirp rate of a ground moving target is approximately equal to that of the clutter because the along-track velocity of a ground moving target is extremely small compared with that of a satellite platform. Therefore we can use the Doppler chirp rate of the clutter to focus the ground moving target echoes. The thin lines shown in Fig. 2 represent the space-time spectrum of a ground moving target. The space-time spectrum of a ground moving target is separated from that of the clutter due to the Doppler frequency shift arising from the cross-track velocity, as shown in Fig. 2. Note that the position of the clutter spectrum in the space-time plane is fixed, while the spectrum of a ground moving target may be at any position depending on its cross-track velocity.

III. PROCESSING APPROACH

We first give the definition of spectrum component which is used extensively in the following.

DEFINITION The space-time spectrum lines shown in Fig. 2(b) can be divided into many short segments (chips) by using the azimuth FFT, each of which is defined as a spectrum component (i.e., spectrum chips) in this paper, such as those in the circles marked in Fig. 2(b).

The proposed approach first extracts all spectrum components (including those of the clutter and ground moving targets) from the space-time plane as shown in Fig. 2(b) by means of space-time beamforming (in practice, the spatial beamforming and temporal beamforming are performed separately). Thus, the spectrum components of ground moving targets can be separated from those of the clutter. Then the resolved clutter spectrum components are rearranged to obtain the unambiguous full spectrum of the clutter as shown by the thick line in Fig. 2(a), and the resolved spectrum components of ground moving targets are also rearranged to obtain the full spectra of ground moving targets as shown by the thin line in Fig. 2(a). Finally, the wide-swath and high-resolution SAR image can be obtained from the unambiguous clutter full spectrum by using conventional SAR imaging operations. To improve the output signal-to-noise ratio (SNR), the full spectra of ground moving targets can also be processed by using SAR imaging operations followed by constant-false-alarm-rate (CFAR) operation. The basic procedures are illustrated in Fig. 3.

The proposed approach is comprised of the following four steps.

Step 1 Temporal Processing

This step divides the echoes received by each satellite into many space-time spectrum components (i.e., spectrum chips), which is necessary to the following spatial processing.

An azimuth FFT is used to divide the echoes received by each satellite into many spectrum components. Within each Doppler bin, each of the spectrum components (including those of the clutter and ground moving targets) is confined into a narrow angle space. Moreover, these spectrum components are completely separated from each other in the spatial domain (angle domain). In the example shown in Fig. 2(b), there are five spectrum components of the clutter and five ones of a ground moving target within each Doppler bin.

As given in (16), the spectra of all clutter cells (within the same range bin) are superimposed in the space-time plane after performing the azimuth FFT, with linear phase differences corresponding to their along-track positions. That is, these clutter cells within each spectrum component have an identical array steering vector. As a result, the spatial processing of each spectrum component is equivalent to processing all the clutter cells within this spectrum component, which is one of the reasons why the approach is more efficient.

No other processing needs to be performed before the azimuth FFT. The SAR imaging operations (such as range migration compensation, range compression, etc.) will be performed after the unambiguous full spectra of the clutter and ground moving targets are retrieved.

Step 2 Spatial Processing

This step extracts all spectrum components from the space-time plane.

Spatial beamforming techniques are used to extract all spectrum components from the space-time plane. To extract a clutter spectrum component, we steer the array mainlobe (i.e., the array steering vector) to the direction of the clutter spectrum component and place nulls in the directions of all the other clutter spectrum components within the corresponding Doppler bin; thus the desired clutter spectrum component can be extracted. The other clutter spectrum components within this Doppler bin can also be extracted by using the same method. Similarly, to extract a spectrum component located in the ground moving target region, the array mainlobe is steered to it and all the clutter spectrum components within the corresponding Doppler bin are nulled out; thus the desired moving target spectrum component can be extracted. To extract a spectrum component, we only need to constrain the array beam pattern in the five or six spectrum component directions within the corresponding range-Doppler bin, which can be easily realized even for a highly sparse satellite array. Because the coherent processing is required in the following steps, the phase and amplitude information of all the spectrum components must be kept unchanged in this step. The way to preserve the phase and amplitude information of all the resolved spectrum components will be detailed in the following.

In the example shown in Fig. 2(b), within each range-Doppler bin there are five clutter spectrum components and five spectrum components of a ground moving target, and each spectrum component comes from a different cone angle. The array steering vectors of the clutter and ground moving target spectrum components can be given by

$$\mathbf{p}_c^i(\tau, f_d) = \left[1, e^{j(4\pi/\lambda)d_{c,2}(\tau, f_d + if_r)}, \ldots, e^{j(4\pi/\lambda)d_{c,M}(\tau, f_d + if_r)}\right]^{\mathrm{T}} \tag{38}$$

and

$$\mathbf{p}_t^i(\tau, f_d) = \left[1, e^{j(4\pi/\lambda)d_{t,2}(\tau, f_d + if_r)}, \ldots, e^{j(4\pi/\lambda)d_{t,M}(\tau, f_d + if_r)}\right]^{\mathrm{T}} \tag{39}$$

respectively, where $i = -I, -I+1, \ldots, I-1, I$ ($2I$ is the number of the Doppler ambiguities), f_r ($-f_r/2 \le f_d < f_r/2$) is the PRF, and $(\cdot)^{\mathrm{T}}$ denotes the vector transpose operator.

The weighted sum of the array signal of the range-Doppler bin $\tau - f_d$ can be formulated as

$$\sum_{m=1}^{M} w_m^*(\tau, f_d) \cdot S_m(\tau, f_d) = \mathbf{w}^{\mathrm{H}}(\tau, f_d) \cdot \mathbf{s}(\tau, f_d) \tag{40}$$

where

$$\mathbf{s}(\tau, f_d) = [S_1(\tau, f_d), S_2(\tau, f_d), \ldots, S_M(\tau, f_d)]^{\mathrm{T}},$$

$\mathbf{w}(\tau, f_d) = [w_1(\tau, f_d), w_2(\tau, f_d), \ldots, w_M(\tau, f_d)]^{\mathrm{T}}$ and $(\cdot)^{\mathrm{H}}$ denotes the vector conjugate-transpose operator. $\mathbf{s}(\tau, f_d)$ is the array output vector (also called the Doppler spectrum vector here) from the range-Doppler bin $\tau - f_d$ and $\mathbf{w}(\tau, f_d)$ is the array weight vector corresponding to the range-Doppler bin $\tau - f_d$. The optimum array weight vector $\mathbf{w}^i(\tau, f_d)$ for extracting the spectrum component i from the range-Doppler bin $\tau - f_d$ can be found by solving the following optimization (Capon beamformer) [20]:

$$\min_{\mathbf{w}} \mathbf{w}^i(\tau, f_d)^{\mathrm{H}} \mathbf{R}(\tau, f_d) \mathbf{w}^i(\tau, f_d) \tag{41}$$

subject to

$$\mathbf{w}^i(\tau, f_d)^{\mathrm{H}} \mathbf{p}_{c[t]}^i(\tau, f_d) = 1 \tag{42}$$

where

$$\mathbf{R}(\tau, f_d) = E\{\mathbf{s}(\tau, f_d)\mathbf{s}^{\mathrm{H}}(\tau, f_d)\} \tag{43}$$

and $\mathbf{R}(\tau, f_d)$ is the covariance matrix corresponding to the array output vector from the range-Doppler bin $\tau - f_d$, and $E\{\}$ denotes the statistical averaging. In practice, $\mathbf{R}(\tau, f_d)$ can be estimated from the sample covariance matrix, and the samples can be easily obtained from range bins (i.e., range samples). The sample covariance matrix $\hat{\mathbf{R}}(\tau, f_d)$ can be

computed by

$$\hat{\mathbf{R}}(\tau, f_d) = \frac{1}{2L+1} \sum_{l=0}^{2L} \mathbf{s}(\tau - L + l, f_d)\mathbf{s}^{\mathrm{H}}(\tau - L + l, f_d) \tag{44}$$

where $2L + 1$ is the number of independent and identically distributed (IID) samples used to estimate the covariance matrix. Reed, et al. have shown that $2L + 1 \geq 2M - 1$ is a rule for a 3 dB loss due to estimation [21].

Solving the optimization of (41) subject to (42), we can obtain the approximately optimum adaptive weight vector $\hat{\mathbf{w}}(\tau, f_d)$ as

$$\hat{\mathbf{w}}^i(\tau, f_d) = \hat{\mathbf{R}}^{-1}(\tau, f_d)\mathbf{p}^i_{c[t]}(\tau, f_d). \tag{45}$$

One major advantage of the array weight obtained by (45) is that it can preserve the phase and amplitude information of each extracted spectrum component. That is, it does not change the phase and amplitude relationships between all the extracted spectrum components.

To compute the optimum array weight vectors for extracting the spectrum components of ground moving targets using (45), the array steering vectors should be known exactly. Unfortunately, in practice the velocities of ground moving targets are usually unknown, so the array steering vectors of the ground moving target spectrum components are also unknown as indicated by (27). If the array steering vectors used to compute the weight vectors mismatch the real ones, the spectrum components may fall into the extensive notches in the beam pattern of the highly sparse array. However, this problem can be mitigated by searching the typical velocity range (or the whole moving target region in the space-time plane shown in Fig. 2(b)); i.e., for each possible velocity (or each possible position in the space-time plane), we use a different array weight vector. Of course, the computation load will be increased.

Step 3 Rearranging Spectrum Components

After all the spectrum components (including those of the clutter and ground moving targets) are extracted, they are then rearranged together to form two kinds of full spectra as shown in Fig. 3, i.e., the unambiguous clutter full spectrum and ground moving target full spectra. The full spectrum vectors of the clutter and ground moving targets can be expressed as

$$\begin{aligned}\mathbf{A}_c(\tau) = \big[&A_c(\tau, -I \cdot f_r), \ldots, A_c(\tau, -f_r), \ldots, A_c(\tau, 0), \ldots, \\ &A_c(\tau, f_r), \ldots, A_c(\tau, I \cdot f_r)\big]^{\mathrm{T}}\end{aligned} \tag{46}$$

and

$$\begin{aligned}\mathbf{A}_t(\tau) = \big[&A_t(\tau, -I \cdot f_r), \ldots, A_t(\tau, -f_r), \ldots, A_t(\tau, 0), \ldots, \\ &A_t(\tau, f_r), \ldots, A_t(\tau, I \cdot f_r)\big]^{\mathrm{T}}\end{aligned} \tag{47}$$

respectively. Moreover, the virtual PRF should be increased up to $2I + 1$ times of the original PRF. The full spectra can be further processed by using conventional SAR imaging operations.

Step 4 Conventional SAR Processing

The full spectra obtained in step 3 will be processed by using conventional SAR imaging operations [22–26], such as range migration compensation, range compression, azimuth compression, etc. By processing the unambiguous clutter full spectrum, we can obtain a full resolution SAR image of wide ground scene. Similarly, we can also obtain SAR images of ground moving targets by processing the full spectra of ground moving targets. To detect ground moving targets, CFAR techniques should be used. In practice, the detected ground moving targets may need to be relocated and marked on the SAR image of ground scene.

In this paper we also perform SAR imaging of the full spectra of ground moving targets after they are separated from that of the clutter. For constellation SAR systems, both the transmitting antenna aperture and transmitted signal power are generally small, so long time coherent integration is necessary to improve the output SNR. Otherwise the detection performance will be very poor due to the high noise level. Additionally, the long time coherent integration can also improve the output signal-to-clutter ratio (SCR) due to the improved azimuth resolution, thus further improving the detection performance. For the above reasons, SAR imaging of ground moving target signals is also performed.

IV. ARRAY ERROR ESTIMATION

In the previous section we presented the data processing technique for resolving the Doppler ambiguity and suppressing the clutter, where we assume that there are no array errors (i.e., the array steering vectors are known accurately). However, the presence of array errors is unavoidable in practice, particularly for such a highly sparse satellite array. These array errors may include the inherent element gain-phase error, beam pattern difference, timing uncertainty, and position uncertainty. To apply the above data processing approach in real system, these errors must be estimated and compensated. In fact, the adaptive processing approach in the previous section can easily compensate the inherent gain error and pattern difference due to the fact that the array weights are adaptively computed for each range-Doppler bin corresponding to a small portion of beam patterns. For narrowband signal, the timing uncertainty can be modeled as a constant phase factor which can be combined with the inherent phase error. Therefore, we only need to consider the array element phase and position errors in this section.

In this section an array auto-calibration technique is proposed to estimate the array errors from the clutter echoes. Recalling the processing approach in the previous section, we do not need to know these individual errors separately in practice, but the array steering vector errors. In other words, the objective of this section is to estimate the array steering vector errors.

As discussed in Section II, the clutter spectrum distributes along the thick lines as shown in Fig. 2(b). Within each range-Doppler bin, there are $2I + 1$ spectrum components of the clutter (in this example, $2I + 1 = 5$) and these spectrum components have different azimuth angles $\theta_c(\tau, f_d + if_r)$ $(i = -I, \ldots, +I)$ and identical incidence angles $\varphi_c(\tau)$. It is the clutter spectrum components within a range-Doppler bin $\tau - f_d$ that are used as the calibration sources in this section. An advantage of using these clutter spectrum components as the calibration sources is that their azimuth angles $\theta_c(\tau, f_d + if_r)$ and incidence angles $\varphi_c(\tau)$ are known; i.e., the calibration sources are in known locations. Therefore, the benefits of source-calibration techniques can be used to develop a fast and robust algorithm to estimate the array errors. Since the clutter spectrum components are different from the conventional calibration sources which are often used in the field of array calibration, we refer to them as "virtual" sources.

A. Error Model

Assume that the true and measured coordinates of the mth satellite are (x_m, y_m, z_m) and (x_{mo}, y_{mo}, z_{mo}), respectively, and the corresponding errors are $(\Delta x_m, \Delta y_m, \Delta z_m)$. Thus the relation between them can be given by

$$(x_m, y_m, z_m) = (x_{mo}, y_{mo}, z_{mo}) + (\Delta x_m, \Delta y_m, \Delta z_m). \tag{48}$$

The unknown errors to be estimated for each array element (satellite) include three position errors $(\Delta x_m, \Delta y_m, \Delta z_m)$ $((\Delta x_1, \Delta y_1, \Delta z_1) = (0,0,0))$ and one gain-phase error (the gain error is also included for completeness in the error model). To estimate all these errors individually, the number of calibration sources must be at least four. However, as mentioned above, we only need to obtain the array steering vector errors, not the individual errors; thus the number of the required calibration sources can be reduced.

Considering the gain-phase error at each array element and the Doppler ambiguities, we rewrite the range-Doppler output (no ground moving target signals) as

$$S_m(\tau, f_d) = g_m e^{j\zeta_m} \sum_{i=-I}^{I} e^{j4\pi d_{c,m}(\tau, f_d + if_r)/\lambda} A_c(\tau, f_d + if_r) + n_m(\tau, f_d) \tag{49}$$

where $g_m e^{j\zeta_m}$ is the gain-phase error of the mth array element.

To simplify the following expressions, we use notations θ^i, φ, d_m^i, S_m, A^i, and n_m to substitute for $\theta_c(\tau, f_d + if_r)$, $\varphi_c(\tau)$, $d_{c,m}(\tau, f_d + if_r)$, $S_m(\tau, f_d)$, $A_c(\tau, f_d + if_r)$, and $n_m(\tau, f_d)$, respectively.

The azimuth angle θ^i of the ith spectrum component can be decomposed into the following two parts:

$$\theta^i = \theta_o + \Delta\theta^i \tag{50}$$

where θ_o ($\theta_o = 0$ in the side-looking mode) is the azimuth angle of the beam center and $\Delta\theta^i$ is the offset of θ^i from the beam center. In practical cases, the antenna beamwidth is very narrow, for example, 0.86° for an antenna with the azimuth length of 2 m at X-band, i.e., $|\Delta\theta^i| < 0.43^\circ$. Assume that the measured relative position errors Δx_m, Δy_m, Δy_m are only tens of centimeters (the accuracy can be easily obtained even by GPS). Under the practical considerations above, we can further rewrite d_m^i as

$$\begin{aligned} d_m^i &= (x_{mo} + \Delta x_m)\sin\theta^i \sin\varphi + (y_{mo} + \Delta y_m)\cos\theta^i \sin\varphi \\ &\quad + (z_{mo} + \Delta z_m)\cos\varphi \\ &\approx d_{mo}^i + \Delta d_m + \Delta d_m^i \end{aligned} \tag{51}$$

where

$$d_{mo}^i = x_{mo}\sin\theta^i \sin\varphi + y_{mo}\cos\theta^i \sin\varphi + z_{mo}\cos\varphi \tag{52}$$

$$\Delta d_m = \Delta x_m \sin\theta_o \sin\varphi + \Delta y_m \cos\theta_o \sin\varphi + \Delta z_m \cos\varphi \tag{53}$$

$$\Delta d_m^i = (\Delta x_m \cos\theta_o - \Delta y_m \sin\theta_o)\sin\Delta\theta^i \sin\varphi. \tag{54}$$

We decompose d_m^i into the three components with the purpose that we can obtain them individually using different methods. d_{mo}^i is the known component that can be directly obtained according to the measured positions, while Δd_m and Δd_m^i are the unknown components to be estimated. Δd_m is constant (i.e., it does not change with the Doppler frequency) in the beam mainlobe in azimuth; thus, it can be modeled as a component of the array element phase error. However, Δd_m^i changes with the Doppler frequency; i.e., it must be estimated for different Doppler frequency, respectively.

Assuming the relative position errors less than 40 cm, i.e., $|\Delta x_m, \Delta y_m, \Delta z_m| < 20$ cm (equivalent phase center), they will introduce the maximum phase error of 36° at X-band. Thus, $e^{j4\pi\Delta d_m^i/\lambda}$ can be expanded as follows (in fact, higher accuracy can still be achieved after several iterations):

$$\begin{aligned} e^{j(4\pi/\lambda)\Delta d_m^i} &\approx 1 + j\frac{4\pi}{\lambda}\Delta d_m^i \\ &= 1 + j\frac{4\pi(\Delta x_m \cos\theta_o - \Delta y_m \sin\theta_o)\sin\varphi}{\lambda}\sin\Delta\theta^i. \end{aligned} \tag{55}$$

Using (51)–(55) in (49) gives

$$S_m = g_m e^{j\zeta_m + j(4\pi\Delta d_m/\lambda)} \sum_{i=-I}^{I} e^{j4\pi d^i_{mo}/\lambda} \left(1 + j\frac{4\pi\Delta d^i_m}{\lambda}\right) A^i + n_m. \tag{56}$$

We can see from (56) that Δd_m is also treated as an array element phase error component. The error term arising from $\Delta x_m \cos\theta_o - \Delta y_m \sin\theta_o$ is transformed into a linear term by using the two-order Taylor-series expansion above. Thus, we can easily obtain the optimum solution of $\Delta x_m \cos\theta_o - \Delta y_m \sin\theta_o$ by using fast algorithms. After the above simplification, now we only need to estimate two errors: the gain-phase error and $\Delta x_m \cos\theta_o - \Delta y_m \sin\theta_o$. Because Δd_m may change slowly with range bins due to the change of the incidence angle φ, in practice we can divide the swath range into multiple short segments and assume Δd_m fixed for each range segment; i.e., we estimate $e^{j\xi_m + j4\pi\Delta d_m/\lambda}$ separately for each range segment.

The array output from the range-Doppler bin $\tau - f_d$, i.e. (56), can be expressed using vector notation as follows:

$$\mathbf{s} = \mathbf{\Gamma P a} + \mathbf{n} \tag{57}$$

where

$$\mathbf{s} = [S_1, S_2, \ldots, S_M]^{\mathrm{T}} \tag{58}$$

$$\mathbf{\Gamma} = \mathrm{diag}\{g_1 e^{j\zeta'_1}, g_2 e^{j\zeta'_2}, \ldots, g_M e^{j\zeta'_M}\} \tag{59}$$

$$\mathbf{P} = [\mathbf{p}^{-I}, \mathbf{p}^{-I+1}, \ldots, \mathbf{p}^{I}] \tag{60}$$

$$\mathbf{a} = [A^{-I}, A^{-I+1}, \ldots, A^{I}]^{\mathrm{T}} \tag{61}$$

$$\mathbf{n} = [n_1, n_2, \ldots, n_M]^{\mathrm{T}} \tag{62}$$

$$\mathbf{p}^i = \left[1, e^{j4\pi d^i_{2o}/\lambda}\left(1 + j\frac{4\pi\Delta d^i_2}{\lambda}\right), \ldots, e^{j4\pi d^i_{Mo}/\lambda}\left(1 + j\frac{4\pi\Delta d^i_M}{\lambda}\right)\right]^{\mathrm{T}} \tag{63}$$

$$\zeta'_m = \zeta_m + \frac{4\pi\Delta d_m}{\lambda}. \tag{64}$$

Assuming the additive noise at each array element is independent and white, the covariance matrix of (57) can be formulated as

$$\mathbf{R_{ss}} = E\{\mathbf{ss}^{\mathrm{H}}\} = \mathbf{\Gamma P R_{aa} P}^{\mathrm{H}} \mathbf{\Gamma}^{\mathrm{H}} + \sigma_n^2 \mathbf{\Sigma}_0 \tag{65}$$

where

$$\mathbf{R_{aa}} = E\{\mathbf{aa}^{\mathrm{H}}\} \tag{66}$$

$$\mathbf{R_{nn}} = E\{\mathbf{nn}^{\mathrm{H}}\} = \sigma_n^2 \mathbf{\Sigma}_0 \tag{67}$$

and σ_n^2 is the noise power and $\mathbf{\Sigma}_0$ is the identity matrix. In practice, we use the sample covariance matrix to estimate the statistical covariance matrix $\mathbf{R_{ss}}$, as given by (44). We can obtain the samples from either the range bins or the same Doppler bin of different pulses.

B. Error Estimation Algorithm

As mentioned above, we only need to estimate two error components, namely, the array element gain-phase error and $\Delta x_m \cos\theta_o - \Delta y_m \sin\theta_o$.

The estimation algorithm is based on the eigen-decomposition of the covariance matrix $\mathbf{R_{ss}}$. Moreover, assume that the eigenvalue decomposition meets the following assumptions.

1) The eigenvalues λ_m $(m = 1, 2, \ldots, M)$ meet $\lambda_1 > \lambda_2 > \cdots > \lambda_{2I+1} \gg \lambda_{2I+2} = \cdots = \lambda_M = \sigma_n^2$, and $\mathbf{u}_m$ is the eigenvector associated with the eigenvalue λ_m.

2) Each column of $\mathbf{B} \triangleq \mathbf{\Gamma P}$ is orthogonal to each column of matrix $\mathbf{U} = [\mathbf{u}_{2I+2}, \mathbf{u}_{2I+3}, \ldots, \mathbf{u}_M]$.

The estimate algorithm comprises two steps. In the first step, fixing Δd^i_m (initial value is zero), we estimate the gain-phase error $g_m e^{j\zeta'_m}$ of each array element. In the second step, using the result of the first step, i.e., holding the gain-phase error fixed, we estimate $\Delta x_m \cos\theta_o - \Delta y_m \sin\theta_o$. The algorithm iterates alternatively between the two steps to find the final solution, as summarized below.

Step 1 Estimating the gain-phase error [18]

Definition of cost function:

$$J_c = \sum_{i=-I}^{I} \|\hat{\mathbf{U}}^{\mathrm{H}} \mathbf{\Gamma p}^i\| \tag{68}$$

where $\hat{\mathbf{U}}$ represents the estimate of the matrix $\mathbf{U}$. If $\hat{\mathbf{U}}$ were a perfect estimate of $\mathbf{U}$ then the minimum value of J_c would be achieved for the true $\mathbf{\Gamma}$ and $\mathbf{p}^i$. Thus, the minimization of J_c can provide estimates of $\mathbf{\Gamma}$ (i.e., $g_m e^{j\zeta'_m}$) and $\mathbf{p}^i$ (i.e., $\Delta x_m \cos\theta_o - \Delta y_m \sin\theta_o$).

The estimate of $\mathbf{\Gamma}$ can be obtained by minimizing the cost function J_c:

$$\begin{aligned}\min_{\mathbf{\Gamma}}(J_c) &= \min_{\mathbf{\Gamma}} \left\{ \sum_{i=-I}^{I} \mathbf{p}^{i\mathrm{H}} \mathbf{\Gamma}^{\mathrm{H}} \hat{\mathbf{U}} \hat{\mathbf{U}}^{\mathrm{H}} \mathbf{\Gamma p}^i \right\} \\ &= \min_{\boldsymbol{\delta}} \left\{ \sum_{i=-I}^{I} \boldsymbol{\delta}^{\mathrm{H}} \mathbf{Q}^{i\mathrm{H}} \hat{\mathbf{U}} \hat{\mathbf{U}}^{\mathrm{H}} \mathbf{Q}^i \boldsymbol{\delta} \right\} \\ &= \min_{\boldsymbol{\delta}} \left\{ \boldsymbol{\delta}^{\mathrm{H}} \left[\sum_{i=-I}^{I} \mathbf{Q}^{i\mathrm{H}} \hat{\mathbf{U}} \hat{\mathbf{U}}^{\mathrm{H}} \mathbf{Q}^i \right] \boldsymbol{\delta} \right\}\end{aligned} \tag{69}$$

where

$$\boldsymbol{\delta} = [\Gamma_{11}, \Gamma_{22}, \ldots, \Gamma_{MM}]^{\mathrm{T}} \tag{70}$$

$$\mathbf{Q}^i = \mathrm{diag}\{\mathbf{p}^i\}. \tag{71}$$

and $\mathrm{diag}\{\mathbf{p}^i\}$ denotes a diagonal matrix whose diagonal is the vector $\mathbf{p}^i$. To place the unknown parameters at the most outer sides of the above expression, the equation $\mathbf{\Gamma p}^i = \mathbf{Q}^i \boldsymbol{\delta}$ is used in (69). Therefore, the optimum solution of the above quadratic minimization problem under linear

constraint $\boldsymbol{\delta}^{\mathrm{H}}\mathbf{w} = 1$ (where $\mathbf{w} = [1,0,0,\ldots,0]^{\mathrm{T}}$) can be directly obtained by

$$\boldsymbol{\delta} = \mathbf{Z}^{-1}\mathbf{w}/(\mathbf{w}^{\mathrm{T}}\mathbf{Z}^{-1}\mathbf{w}) \tag{72}$$

where

$$\mathbf{Z} \triangleq \sum_{i=-I}^{I} \mathbf{Q}^{i\mathrm{H}}\hat{\mathbf{U}}\hat{\mathbf{U}}^{\mathrm{H}}\mathbf{Q}^{i}. \tag{73}$$

Then the gain-phase errors $g_m e^{j\zeta'_m}$ are given by

$$\boldsymbol{\Gamma} = \mathrm{diag}(\boldsymbol{\delta}). \tag{74}$$

Thus, we can compensate the gain-phase error (including the inherent gain-phase error and those arising from the timing and relative position uncertainties) at each array element according to the diagonal element of $\boldsymbol{\Gamma}$.

We usually choose the clutter spectrum components in the Doppler center bin (i.e., $f_d = 0$ in the side-looking mode) as the calibration sources. From the computer simulations we find that even if we ignore the effect of $\Delta x_m \cos\theta_o - \Delta y_m \sin\theta_o$ (i.e., assume $\Delta x_m \cos\theta_o - \Delta y_m \sin\theta_o = 0$ in the first step), the estimate accuracy of the phase error $e^{j\zeta'_m}$ is still satisfactory (less than 1°). Furthermore, to further reduce the effect of noise, we can average the estimates obtained from other Doppler bins.

Step 2 Estimating $\Delta x_m \cos\theta_o - \Delta y_m \sin\theta_o$

Holding $\boldsymbol{\Gamma}$ fixed, we then estimate $\Delta x_m \cos\theta_o - \Delta y_m \sin\theta_o$.

The array steering vectors $\mathbf{p}^i$ of the calibration sources can be decomposed into the following two parts:

$$\mathbf{p}^i = \mathbf{p}_0^i + \mathbf{P}_1^i \boldsymbol{\Delta}\mathbf{d} \tag{75}$$

where

$$\mathbf{p}_0^i = \left[1, e^{j4\pi d^i_{2o}/\lambda}, \ldots, e^{j4\pi d^i_{Mo}/\lambda}\right]^{\mathrm{T}} \tag{76}$$

$$\mathbf{P}_1^i = \mathrm{diag}\left\{1, j\frac{4\pi \sin\Delta\theta^i \sin\varphi}{\lambda} e^{j4\pi d^i_{2o}/\lambda}, \ldots, j\frac{4\pi \sin\Delta\theta^i \sin\varphi}{\lambda} e^{j4\pi d^i_{Mo}/\lambda}\right\} \tag{77}$$

$$\boldsymbol{\Delta}\mathbf{d} = \left[0, \Delta x_2 \cos\theta_o - \Delta y_2 \sin\theta_o, \ldots, \Delta x_M \cos\theta_o - \Delta y_M \sin\theta_o\right]^{\mathrm{T}}. \tag{78}$$

We rewrite the cost function of (68) as follows:

$$J_c = \|\mathbf{E} - \mathbf{F}\Delta\mathbf{d}\| \tag{79}$$

where

$$\mathbf{E} = [\mathbf{e}_{-I}^{\mathrm{T}} \ \mathbf{e}_{-I+1}^{\mathrm{T}} \cdots \mathbf{e}_{I}^{\mathrm{T}}]^{\mathrm{T}} \tag{80}$$

$$\mathbf{F} = [\mathbf{f}_{-I}^{\mathrm{T}} \ \mathbf{f}_{-I+1}^{\mathrm{T}} \cdots \mathbf{f}_{I}^{\mathrm{T}}]^{\mathrm{T}} \tag{81}$$

$$\mathbf{e}_i = \hat{\mathbf{U}}^{\mathrm{H}}\boldsymbol{\Gamma}\mathbf{p}_0^i \tag{82}$$

$$\mathbf{f}_i = -\hat{\mathbf{U}}^{\mathrm{H}}\boldsymbol{\Gamma}\mathbf{P}_1^i. \tag{83}$$

The least square solution of (79) can be obtained by

$$\Delta\mathbf{d} = \mathrm{real}\{(\mathbf{F}^{\mathrm{H}}\mathbf{F})^{-1}\mathbf{F}^{\mathrm{H}}\mathbf{E}\}. \tag{84}$$

If the accuracy of Taylor-series expansion of (55) cannot meet practical requirements, however, much higher estimation accuracy will be achieved by increasing iteration number, and this can also further mitigate the rigorous requirement on the measurement accuracy.

The optimum estimates of $g_m e^{j\zeta'_m}$ and $\Delta x_m \cos\theta_o - \Delta y_m \sin\theta_o$ can be directly obtained by (72) and (84). Therefore the computational burden is reduced significantly.

V. SATELLITE FORMATION OPTIMIZATION

To retrieve the unambiguous full clutter spectrum from the Doppler-ambiguous ground echoes by using the processing approach in Section III, the satellite arrays must meet some constraints. This section is to investigate the array configuration requirements.

Throughout this paper, a satellite array with very short cross-track baselines (on the order of 10 m) is assumed. In fact, if the illuminated ground surface is flat or it can be known accurately, the proposed approaches can still apply to an array with long cross-track baselines. However, the illuminated ground terrain is usually not flat and usually not known accurately, which means that the array steering vectors of spectrum components are also unknown for an array with long cross-track baselines. Another problem introduced by an array with long cross-track baselines is the envelope coregistration in the presence of Doppler ambiguities. Therefore, the processing approaches suffer seriously from a large three-dimensional array. The shorter the cross-track baselines, the less effect of a rugged terrain. For such a reason, a sparse linear array (with very short cross-track baselines) in along-track direction relative to the ground is the ideal formation for SAR mapping and GMTI applications. However, even for an along-track sparse linear array, there are still some configuration constraints that must be satisfied for retrieving the unambiguous full clutter spectrum. The mathematical analysis of the array configuration constraints is given in the following.

In fact, x_m can be decomposed into the following two parts:

$$x_m = k_m v_s T_r + \delta x_m \tag{85}$$

where k_m is an integer, T_r is the pulse repetition period, and $-v_s T_r/2 \le \delta x_m < v_s T_r/2$. If y_m and z_m are very small (or even zero), we can rewrite the array steering phase $e^{j4\pi d^i_m/\lambda}$ of the ith clutter spectrum component of the range-Doppler bin $\tau - f_d$ as (using

(85))

$$\begin{aligned} e^{j4\pi d_m^i/\lambda} &= e^{j4\pi/\lambda(x_m \sin\theta^i \sin\varphi + y_m \cos\theta^i \sin\varphi + z_m \cos\varphi)} \\ &= e^{j2\pi(f_d + if_r)(x_m/v_s) + j(4\pi/\lambda)(y_m \cos\theta^i \sin\varphi + z_m \cos\varphi)} \\ &= e^{j2\pi f_d k_m T_r} e^{j(4\pi/\lambda)\delta x_m \sin\theta^i \sin\varphi + j(4\pi/\lambda)(y_m \cos\theta^i \sin\varphi + z_m \cos\varphi)} \\ &\approx e^{j2\pi f_d k_m T_r + j(4\pi/\lambda)(y_m \cos\theta_o \sin\varphi + z_m \cos\varphi)} e^{j(4\pi/\lambda)\delta x_m \sin\theta^i \sin\varphi}. \end{aligned} \tag{86}$$

Note that only the second exponential term in (86) relates to the ith spectrum component. That is, the array steering vectors of clutter spectrum components only depend on δx_m but are independent of $k_m v_s T_r$. Equation (86) means that no matter how long an along-track linear array is, only its equivalent short array with the maximum length of $v_s T_r$ is virtually valid for resolving the Doppler ambiguities. We refer here to the array with the element positions (along-track) of $[0, \delta x_2, \ldots, \delta x_M]$ as the compressed array. Therefore, to evaluate the Doppler ambiguity resolving performance of a large sparse array is equivalent to evaluating that of its corresponding compressed array. Since the compressed array is also a conventional array as indicated by (86), its configuration requirements for resolving sources (i.e., spectrum components in this paper) in different directions are well known; that is, the array elements should be well distributed in the interval $[0, v_s T_r]$.

In practical processing we can firstly delay the pulses received by each satellite in slow time (azimuth time) domain to obtain the compressed array before performing the SAR and GMTI processing in Section III; i.e., the pulses received by the mth satellite are delayed by $k_m T_r$. This is equivalent to changing the along-track position of the satellite from x_m to $\delta x_m = x_m - k_m v_s T_r$.

In fact, the DPCA technique can also be used for GMTI. The DPCA technique requires that the along-track intervals of satellites must be $k_m v_s T_r$ (k_m is an integer). Unfortunately, when the DPCA condition is satisfied, the along-track length of the compressed array is zero (i.e., $\delta x_m = 0$). As discussed above, this kind of satellite formation does not hold the ability to retrieve the unambiguous full clutter spectrum for SAR imaging of ground scenes. Therefore, the DPCA formation is not a good choice.

If a given satellite formation cannot meet the above array configuration requirements, what should we do? A straightforward method is to change the satellite formation by thrusters. Another method is to slightly adjust the PRF. From (85) we can see that δx_m depends not only on x_m, but also on T_r, so we can change δx_m by slightly changing the PRF. For example, assume that the array element positions (along-track) of a given formation are 0 m, 50.0627 m, 100.3473 m, 150.3043 m, 200.4931 m, 250.1518 m, 300.4489 m, 350.2959 m, and 400.2448 m, respectively. For v_s = 7481.5 m/s and f_r = 1496 s (i.e., $v_s T_r$ = 5.001 m), the corresponding element positions (along-track) of the compressed array are 0 m, 0.0526 m, 0.3272 m, 0.2742 m, 0.4529 m, 0.1016 m, 0.3887 m, 0.2257 m, and 0.1646 m, respectively. Because the compressed array is too short (only 0.5 m), it is difficult to resolve the Doppler ambiguities. If the PRF is changed as f_r = 1478 Hz, then the corresponding element positions of the compressed array will become 0 m, 4.5055 m, 4.1710 m, 3.5090 m, 3.0787 m, 2.1183 m, 1.7963 m, 1.0242 m, and 0.3541 m, respectively. Now, the compressed array can satisfy the configuration requirements.

For SAR and GMTI applications, we require the satellite formation be an along-track linear array (or with very short cross-track baselines). Unfortunately, this kind of satellite formation cannot be used to collect the topographic height information. This problem can be solved by two along-track linear arrays with a long cross-track interval between them. The ground echoes received by each linear array are processed separately to produce two wide-swath, high-resolution, complex SAR images of the same ground scene, and then the obtained two complex SAR images can be processed by using the interferometric processing to retrieve the topographic height information [27].

VI. SIMULATED RESULTS

The simulated constellation comprises 9 small satellites, all of which have identical small antennas. In this implementation, one small satellite is used as both illuminator and receiver, while all the other small satellites only receive the echoed signals. We also assume they operate in the side-looking mode. The key simulation parameters of the constellation SAR system are listed in Table I. The measured coordinates of each satellite and the corresponding errors are given in Table II (equivalent phase centers). To verify the ability of the proposed approach to resolve Doppler ambiguities and achieve high quality SAR images, we use a real SAR image (obtained by our airborne SAR system) as the simulated ground scene (flat surface) and generate the clutter return using the parameters listed in Table I. The clutter return from the simulated ground scene is received by all the satellites. In the following we use the clutter to verify the techniques of array auto-calibration and unambiguous SAR mapping of ground scene.

We first verify the performance of the array auto-calibration technique. To estimate the covariance matrix of (65), 200 samples were used. All the samples were obtained from 20 adjacent range bins, with 10 samples obtained from each range bin. The method for obtaining 10 samples from each range bin is described as follows. The total number of pulses

TABLE I
Main Simulation Parameters of Constellation SAR System

Orbit Altitude	Incidence Angle	Band	Antenna Size	Bandwidth	PRF	Satellite Velocity
750 Km	45°	X-band	2 m × 1 m (along-track×cross-track)	100 MHz	1496 Hz	7481.5 m/s

TABLE II
Measured Coordinates and Corresponding Errors

No. of Satellite	Measurement Value x_o (m)	Measurement Value y_o (m)	Measurement Value z_o (m)	Error Δx (m)	Error Δy (m)	Error Δz (m)
1	0	0	0	0	0	0
2	41.0610	2.4275	1.5671	0.2088	−0.2192	0.0395
3	96.5630	0.2871	−2.6572	−0.1014	0.1624	−0.1293
4	145.5115	−3.4532	4.7626	0.1463	−0.1417	0.2149
5	199.0970	1.6433	5.0979	0.2110	0.1179	0.0567
6	252.0825	4.4777	−2.1979	0.0601	0.1295	0.1509
7	307.8350	−3.8661	1.0681	−0.1595	−0.0628	−0.1541
8	354.5835	3.9742	4.4865	−0.0865	0.1168	−0.2013
9	413.3735	−4.5444	−4.8235	0.0346	0.1412	0.1642

used for estimating the covariance matrix is 1519 (i.e., the total azimuth time is about 1.0 s). The length of each azimuth FFT is 1024 (pulses) and the interval between two adjacent FFTs is only 55 pulses (i.e., 969 overlapping pulses). We assume that there is no the inherent gain-phase error (due to the fact that the estimate of $e^{j\zeta_m}$ is the same as the estimate of $e^{j4\pi\Delta d_m/\lambda}$ and the estimate of g_m is unnecessary to the proposed adaptive processing approach) at each array element and the clutter-to-noise ratio (within each Doppler bin) is 10 dB. The estimate results (one trial) of the array auto-calibration technique are shown in Table III. The estimate accuracy is on the order of 1° which can meet our practical requirements.

After estimating and compensating the position errors for each satellite, we then verify the ability of the proposed processing approach to resolve the Doppler ambiguities. Shown in Fig. 4(a) is the result of SAR imaging without compensating the position errors, while shown in Fig. 4(b) is the result with compensating the position errors. Fig. 4(b) demonstrates that the proposed processing approach can recover the unambiguous SAR image of the simulated ground scene. The performance of GMTI is also investigated with the same clutter from the simulated ground scene. A ground moving scatterer is placed in the ground scene with its RCS equal to the average RCS of the clutter SAR pixels (i.e., the input signal-to-clutter ratio is 0 dB) and its cross-track velocity (no along-track velocity) is in the range of [0–25] m/s. The input clutter-to-noise ratio (within the SAR image) is 45 dB (somewhat higher than that in practical systems, for example, 30 dB). The echoes from the simulated ground scene (including the stationary pixels and the moving target) are received by all the satellites. As mentioned in Section III,

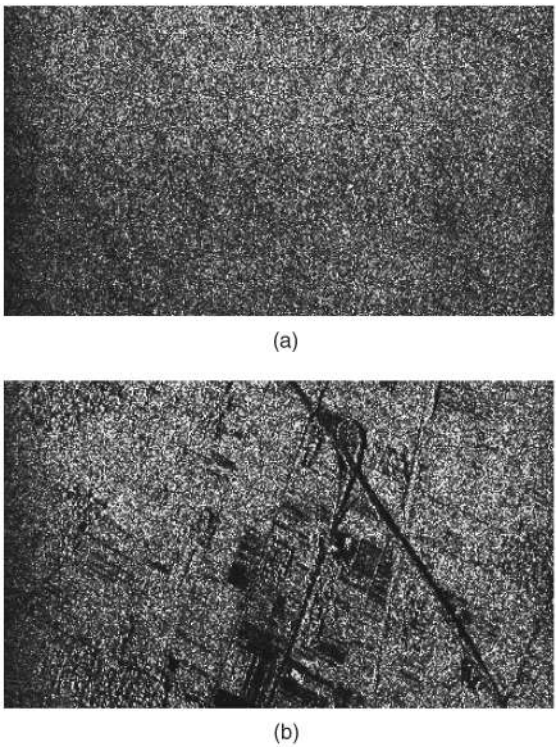

Fig. 4. SAR processing of simulated scene return using proposed approach. (a) Without compensating the position errors. (b) With compensating the position errors.

since the velocities of ground moving targets are usually unknown (i.e., the array steering vectors are unknown), we need to search the whole velocity range (generally [0–60] m/s) for ground moving targets. In this simulation, we search the velocity range of [0–25] m/s at the interval of 0.5 m/s, although we do know the true velocity of the ground moving target. The signal-to-clutter+noise-ratio (SCNR)

TABLE III
Estimates of Position Errors

No. of Satellite	$720\frac{\Delta d_m - \Delta\hat{d}_m}{\lambda}$ (degree)	$720\frac{\Delta d_m^i - \Delta\hat{d}_m^i}{\lambda}$ $(i = 2)$ (degree)
1	0	0
2	0.05	1.48
3	0.20	−1.85
4	0.60	−0.97
5	−0.01	1.19
6	0.88	0.80
7	−0.17	−1.31
8	−0.31	0.83
9	−0.44	−1.58

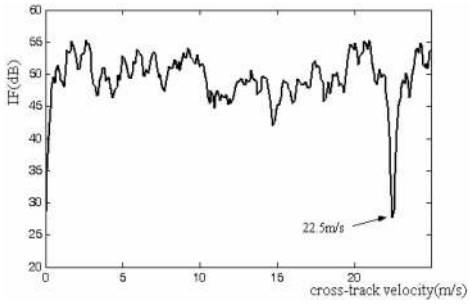

Fig. 5. SCNR improvement factor velocity response.

improvement factor (IF) versus the cross-track velocity is shown as the curve (also referred to as the velocity response) in Fig. 5. The SCNR IF is defined as "the output SCNR of a system divided by the SCNR at the input of the system."

From Fig. 5 we can see that a fine IF curve can be achieved. Note there is a null at the cross-track velocity of 22.5 m/s in Fig. 5. This is because the space-time spectrum of the ground moving target will be at the same position in the space-time plane as the clutter spectrum if the cross-track velocity equals to 22.5 m/s; i.e., they cannot be separated in the space-time plane. This area is referred to as the blind velocity area in literatures. Except the blind velocity area, fine IF can be achieved by using the approach.

VII. CONCLUSIONS

Future spaceborne SAR system will be required to achieve wide area surveillance, not only mapping of wide ground scenes with high resolution but also detecting ground moving targets. The constellation SAR system is a promising choice. However, some problems impede the implementation of constellation SAR systems at present, including range/Doppler ambiguities, highly sparse array signal processing, timing and position uncertainties, etc. In this paper, we use signal processing techniques to solve the problems of high-resolution SAR imaging of wide areas, detection of ground moving targets, array auto-calibration, and satellite formation optimization. The interesting characteristics of the proposed techniques are simplicity, efficiency, and robustness.

ACKNOWLEDGMENT

The authors wish to thank Dr. Hongwei Liu and Ms. Shelley Crawford for revising the English and syntax.

REFERENCES

[1] Das, A., and Cobb, R.
TechSat 21—Space missions using collaborating constellations of satellites.
In *Proceedings of the 12th AIAA/USU Conference on Small Satellites* (SSC98-VI-1), Logan, UT, Aug. 1998, A99-10826-01-20.

[2] Martin, M., and Stallard, M.
Distributed satellite missions and technologies—The TechSat 21 program.
In *Proceeding of AIAA Space Technology Conference and Exposition*, Albuquerque, NM, Sept. 1999, AIAA-99-4479.

[3] Massonnet, D.
Capabilities and limitations of the interferometric cartwheel.
IEEE Transactions on Geoscience and Remote Sensing, **39** (2001), 506–520.

[4] Ramongassie, S., Phalippou, L., Thouvenot, E., and Massonnet, D.
Preliminary design of the payload for the interferometric cartwheel.
In *Proceedings of the International Geoscience and Remote Sensing Symposium 2000*, Honolulu, HI, July 2000, 1004–1006.

[5] Goodman, N. A., Lin, S. C., Rajakrishna, D., and Stiles, J. M.
Processing of multiple-receiver spaceborne arrays for wide-area SAR.
IEEE Transactions on Geoscience and Remote Sensing, **40** (Apr. 2002), 841–852.

[6] Krieger, G., Fiedler, H., Rodriguez-Cassola, M., Hounam, D., and Moreira, A.
System concepts for bi- and multi-static SAR missions.
In *Proceedings of the IEEE International Radar Conference*, Dresden, Germany, Sept. 2003.

[7] Aguttes, J. P.
The SAR train concept: Required antenna area distributed over N smaller satellites, increase of performance by N.
In *Proceedings of the International Geoscience and Remote Sensing Symposium 2003*, Toulouse, France, July 2003, 542–544.

[8] Schindler, J. K., Steyskal, H., and Franchi, P.
Pattern synthesis for moving target detection with TechSat21-A distributed spacebased radar system.
In *Radar 2002*, Edinburgh, UK, Oct. 2002, 375–379.

[9] Marais, K., and Sedwick, R.
Space based GMTI using scanned pattern interferometric radar (SPIR).
In *Proceedings of the 2001 IEEE Aerospace Conference*, Big Sky, MT, Mar. 2001, 4/2047-4/2055.

[10] Hovanessian, S. A., Jocic, L. B., and Lopez, J. M.
Spaceborne radar design equations and concepts.
In *Proceedings of the 1997 IEEE Aerospace Conference*, Snowmass Village, CO, Feb. 1997, 125–136.

[11] Nohara, T. J.
Comparison of DPCA and STAP for space-based radar.
In *Proceedings of the IEEE International Radar Conference*, Alexandria, VA, May 1995, 113–119.

[12] Cantafio, L. J.
Space-Based Radar Handbook.
Boston: Artech House, 1989, 127–132.

[13] Li, F. K., and Johnson, W. T. K.
Ambiguities in spaceborne synthetic aperture radar systems.
IEEE Transactions on Aerospace and Electronic Systems, **19** (May 1983), 389–396.

[14] Tomiyasu, K.
Image processing of synthetic aperture radar range ambiguous signals.
IEEE Transactions on Geoscience and Remote Sensing, **32** (Sept. 1994), 1114–1117.

[15] Bamler, R., and Runge, H.
PRF ambiguity resolving by wavelength diversity.
IEEE Transactions on Geoscience and Remote Sensing, **29** (1991), 997–1003.

[16] Hung, E.
Matrix-construction calibration method for antenna arrays.
IEEE Transactions on Aerospace and Electronic Systems, **36** (2000), 819–828.

[17] Ng, B. C., and Seem, C. M. S.
Sensor-array calibration using a maximum-likelihood approach.
IEEE Transactions on Antennas Propagation, **44** (1996), 827–835.

[18] Friedlander, B., and Weiss, A. J.
Direction finding in the presence of mutual coupling.
IEEE Transactions on Antennas Propagation, **39** (1991), 273–284.

[19] See, C. M. S., and Poh, B. K.
Parametric sensor array calibration using measured steering vectors of uncertain locations.
IEEE Tranactions on Signal Processing, **47** (1999), 1133–1137.

[20] Capon, J.
High resolution frequency-wavenumber spectrum analysis.
Proceedings of the IEEE, **57** (1969), 1408–1418.

[21] Reed, I. S., Mallett, J. D., and Brennan, L. E.
Rapid convergence rate in adaptive arrays.
IEEE Transactions on Aerospace and Electronic Systems, **10** (1974), 853–863.

[22] Moreira, A., Mittermayer, J., and Scheiber, R.
Extended chirp scaling algorithm for air- and spaceborne SAR data processing in stripmap and ScanSAR imaging modes.
IEEE Transactions on Geoscience and Remote Sensing, **34** (Sept. 1996), 1123–1136.

[23] Raney, R. K., Runge, H., Bamler, R., Cumming, I., and Wong, F.
Precision SAR processing using chirp scaling.
IEEE Transactions on Geoscience and Remote Sensing, **32** (July 1994), 786–799.

[24] Cafforio, C., Prati, C., and Rocca, F.
SAR data focusing using seismic migration techniques.
IEEE Transactions on Aerospace and Electronic Systems, **27** (1991), 194–207.

[25] Lanari, R.
A new method for the compensation of the SAR range cell migration based on the chirp Z-transform.
IEEE Transactions on Geoscience and Remote Sensing, **33** (1995), 1296–1299.

[26] Jin, M., and Wu, C.
A SAR correlation algorithm which accommodates large range migration.
IEEE Transactions on Geoscience and Remote Sensing, **22** (1984), 592–597.

[27] Li, F. K., and Goldstein, R. M.
Studies of multibaseline spaceborne interferometric synthetic aperture radars.
IEEE Transactions on Geoscience and Remote Sensing, **28** (Jan. 1990), 88–97.

Zhenfang Li received the B.S. degree in automatization and the M.S. degree in electronic information engineering from Xidian University, China, in 1999 and 2001, respectively.

He is currently pursuing the Ph.D. degree in radar signal processing at the National Lab of Radar Signal Processing at Xidian University. His current research is in SAR and GMTI signal processing of distributed small satellite SAR systems.

Zheng Bao (M'80—SM'90) was born in Jiangsu, China in 1927. He graduated from the Communication Engineering Institute of China in 1953.

Currently, he is a professor at Xidian University. His research fields are space-time adaptive processing (STAP), radar imaging (SAR/ISAR), automatic target recognition (ATR) and over-the-horizon radar (OTHR) signal processing.

Dr. Bao is a member of the Chinese Academy of Sciences. He has authored or coauthored 6 books and published over 300 papers.

Hongyang Wang was born in TianJin, China, in 1976. He received the M.S. and Ph.D. degrees in signal processing in 2001 and 2005, respectively, both from the National Lab of Radar Signal Processing at Xidian University, China.

He is now working at the Chinese University of Hong Kong. His research interests include weak signal detection and space-time signal processing with applications in radar and wireless communication systems.

Guisheng Liao (M'96) received the B.S. degree from Guangxi University, Guangxi, China, in 1985 and the M.S. and Ph.D. degrees from Xidian University, Xi'an, China, in 1990 and 1992, respectively.

He joined the National Lab of Radar Signal Processing at Xidian University in 1992, where he is currently a vice director of the lab. His research interests are mainly in statistical and array signal processing, signal processing for radar and communication, and smart antenna for wireless communication.